Impact of going beyond the Maxwell distribution in direct dark matter detection rates

J. D. Vergados,[1] S. H. Hansen,[2] and O. Host[2]

[1]*University of Cyprus, Nicosia, CY-1678, Cyprus*

[2]*Dark Cosmology Centre, Niels Bohr Institute, University of Copenhagen, Juliane Maries Vej 30, DK-2100 Copenhagen, Denmark*

(Received 10 September 2007; published 14 January 2008)

We consider direct dark matter detection rates and investigate the difference between a standard Maxwell-Boltzmann velocity distribution and a ''realistic'' distribution like the ones extracted from numerical *N*-body simulations. Sizable differences are observed when such results are compared to the standard Maxwell-Boltzmann distribution. For a light target both the total rate and the annual modulation are reduced by ~25%. For a heavy target the total rate is virtually unchanged, whereas the annual modulation is modified by up to 50%, depending on the weakly interacting massive particle mass and detector energy threshold. We also consider the effect of a possible velocity anisotropy, and the effect is found to be largest for a light target. For the realistic velocity distribution the anisotropy may reduce the annual modulation, in contrast to the Maxwell-Boltzmann case.

DOI: 10.1103/PhysRevD.77.023509 PACS numbers: 95.35.+d, 12.60.Jv

I. INTRODUCTION

The Universe is observed to contain large amounts of dark matter [1,2], and its contribution to the total energy density is estimated to be ~25%. This nonbaryonic dark matter component, responsible for the growth of cosmological perturbations through gravitational instability, has still not been detected directly. Even though there exists firm indirect evidence from the halos of dark matter in galaxies and clusters of galaxies it is essential to detect matter directly.

The possibility of direct detection, however, depends on the nature of the dark matter constituents. Supersymmetry naturally provides candidates for these constituents [3–6]. In the most favored scenario of supersymmetry, the lightest supersymmetric particle (LSP) can be described as a Majorana fermion, a linear combination of the neutral components of the gauginos and Higgsinos.

Since the LSPs [or weakly interacting massive particles (WIMPs)] are expected to be very massive ($m_{\mathrm{WIMP}} \gtrsim 30$ GeV) and extremely nonrelativistic with average kinetic energy $\langle T \rangle \simeq 50$ keV $m_{\mathrm{WIMP}}/100$ GeV, a WIMP interaction with a nucleus in an underground detector is not likely to produce excitation. As a result, WIMPs can be directly detected mainly via the recoil of a nucleus (A, Z) in elastic scattering. The event rate for such a process can be computed from the following ingredients:

(1) An effective Lagrangian at the elementary particle (quark) level obtained in the framework of the prevailing particle theory. For supersymmetry this is achieved as described in Refs. [6,7], for example.

(2) A well-defined procedure for transforming the amplitude obtained using the previous effective Lagrangian from the quark to the nucleon level, i.e. a quark model for the nucleon. This step in supersymmetric models is nontrivial, since the obtained results depend crucially on the content of the nucleon in quarks other than u and d.

(3) Knowledge of the relevant nuclear matrix elements [8,9], obtained with reliable many-body nuclear wave functions. Fortunately, in the case of the scalar coupling, which is viewed as the most important, the situation is a bit simpler, as only the nuclear form factor is needed.

(4) Knowledge of the WIMP density in our vicinity and its velocity distribution. Since the essential input here comes from the rotation curves, dark matter candidates other than the LSP are also characterized by similar parameters.

In the past, various velocity distributions have been considered for the dark matter gas in our galaxy. The most popular one is the isothermal Maxwell-Boltzmann (M-B) velocity distribution with $\langle v^2 \rangle = 3v_d^2 \simeq 3v_0^2/2$, where $v_d^2 = \langle v_x^2 \rangle = \langle v_y^2 \rangle = \langle v_z^2 \rangle$ and v_0 is the velocity of the Sun around the galaxy, i.e. $v_0 \simeq 220$ km/s. Extensions of the M-B distribution have also been considered, in particular, those that are axially symmetric with enhanced dispersion in the galactocentric direction [10–13]. The need for such a velocity anisotropy is numerically well founded [14]. It has also been shown that the velocity anisotropy is, in principle, measurable in a direction sensitive experiment [15], and it has possibly been observed to be nonzero in clusters of galaxies [16].

Nonisothermal models have also been considered. Among these one should mention dark matter orbiting the Sun [17], or dark matter which is part of the Sagittarius tidal stream [18]. The velocity distribution has also been obtained in ''adiabatic'' models employing the Eddington method [19–22]. In such an approach, given the density of matter, one can obtain a distribution that depends both on the velocity and the gravitational potential. Evaluating this distribution in a given point in space, e.g. in our vicinity, yields the velocity distribution at that point in a self-consistent manner. Unfortunately this approach is applicable only if the density of matter is spherically symmetric and the distribution depends only on energy.

Also variants of the M-B distribution resulting from a coupling of dark matter to dark energy [23] have been considered.

In the present work we will consider a Tsallis type velocity distribution [24]. This has been found to be a good description of the velocity distributions in numerical simulations with realistic dark matter density and anisotropy profiles [25]. We compare the direct dark matter detection rates obtained in this way with the results for an axially symmetric Maxwell-Boltzmann velocity distribution.

II. A REALISTIC VELOCITY DISTRIBUTION

Let us first introduce and discuss all the details of the velocity distribution function (VDF) which we will use.

Very often the VDF of the dark matter particles is approximated by a Maxwell-Boltzmann shape (a Gaussian). There are many good reasons for doing this, in particular, the fact that many steps can be made analytically since the M-B is easy to integrate. It is, however, well known that the M-B is only an approximation, which is accurate only for an isothermal sphere. For more general density profiles the shape of the VDF has a different form. For example, when considering a power law in density over many orders of magnitude, one finds for isotropic structures that the VDF has the Tsallis shape [26]. The Tsallis VDF depends on a entropic index q in such a way that the normal M-B is the limiting case for $q \to 1$ [24]. The shape of the VDF for more realistic cosmological dark matter structures has still not been calculated analytically, partly because the distribution function cannot be assumed to depend only on energy. First steps in the direction of actually deriving the VDF from a generalized Eddington method have been taken [27].

It has recently been identified that the *shape* of the VDF actually is different for the galactic radial and tangential directions [25]. This means that when the particle velocity is decomposed into the radial and the tangential component with respect to the galactic center, the corresponding distributions are different. Specifically, it appears that the tangential VDF is always well fit with the Tsallis shape using an entropic index of $q = 5/3$, at least for velocities smaller than 1.6 times the velocity dispersion. Thus the tangential VDF is universal at any radius and the only free parameter is the tangential velocity dispersion.

The radial VDF, however, differs strongly as a function of radius. It appears that the form of the radial VDF is fairly similar to what comes out of the Eddington method, when using a density profile of the NFW [28] or Sersic shape [29,30]. In the inner part of the dark matter halo the shape of the radial VDF is fairly simple, and again the shape is reasonably well fit by the Tsallis shape with entropic index fairly close to unity. A clear advantage of approximating the real VDFs by distributions of the Tsallis shape is, as in the Maxwell-Boltzmann case, that certain integrals can be done analytically.

We therefore consider a distribution function in the radial direction which is given by

$$f_r(v, \sigma_r, q) = N(q, \sigma_r)\left(1 - \frac{(1-q)v^2}{(3-q)\sigma_r^2}\right)^{q/1-q}, \qquad v^2 = v_r^2, \tag{1}$$

where σ_r is the radial velocity dispersion and $N(q, \sigma_r)$ is a normalization factor. We note that

$$\left(1 - \frac{(1-q)v^2}{(3-q)\sigma_r^2}\right)^{q/1-q} \to \exp\left(-\frac{v^2}{2\sigma_r^2}\right) \quad \text{as } q \to 1.$$

For $q > 1$ this function is defined on the whole axis. For $q < 1$ the domain is limited, since one must demand that the function is nonnegative. Thus for $q = 3/4$ the function becomes

$$f_r(v, \sigma_r) = \frac{35}{96\sigma_r}\left(1 - \frac{v^2}{9\sigma_r^2}\right)^3, \qquad -3\sigma_r \le v \le 3\sigma_r. \tag{2}$$

We emphasize that this distribution thus automatically imposes an upper bound on the acceptable velocities. In the case of the M-B distribution this is imposed by hand, $v_{\rm esc} = 2.84 v_0$, where v_0 is the solar rotational velocity.

The corresponding Maxwell-Boltzmann distribution, i.e. the limit of (1) as $q \to 1$, is given by

$$f_{\rm MB}(v, \sigma_r) = \frac{1}{\sqrt{2\pi}\sigma_r} \exp\left(-\frac{v^2}{2\sigma_r^2}\right). \tag{3}$$

Both the Tsallis shape with $q = 3/4$ and the M-B shape (corresponding to $q = 1$) are shown in Fig. 1.

The tangential velocity distribution, defined and normalized in two dimensions, is characterized by $q > 1$ and takes the form

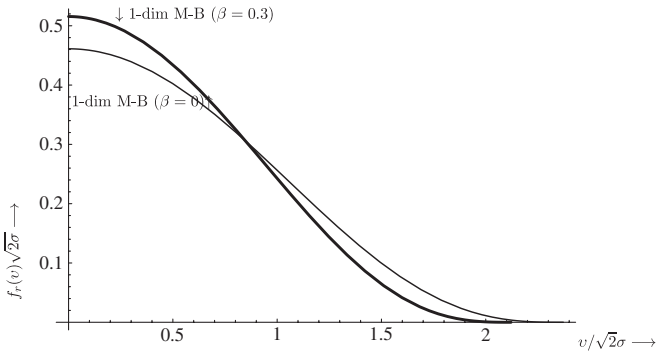

FIG. 1. The normalized velocity distribution in the radial direction $f_r(v)\,(v = v_r)$ for $\beta = 0$ as a function of $v/\sigma\sqrt{2}$ for $q = 3/4$ (thin line) and the one-dimensional M-B distribution (thick line). For $\beta = 0$, $\sigma = \sigma_r$. Since this one-dimensional distribution is symmetric, only the sector $v \ge 0$ is shown.

$$f_t(v,\sigma_t)=\frac{1}{2\pi\sigma_t^2(2-q)}\left(1-\frac{q-1}{2(q-2)}\left(\frac{v}{\sigma_t}\right)^2\right)^{q/1-q},\qquad v^2=v_t^2. \tag{4}$$

Introducing the asymmetry parameter β defined by

$$\beta=1-\frac{\sigma_t^2}{\sigma_r^2}, \tag{5}$$

and using the relation for the total velocity dispersion

$$3\sigma^2=\sigma_r^2+2\sigma_t^2, \tag{6}$$

we can express this distribution in terms of β and σ. Thus we obtain

$$f_t(v,\beta,\sigma)=\frac{1}{2\pi\sigma^2(2-q)}\frac{1-\frac{2}{3}\beta}{1-\beta}\times\left(1-\frac{(q-1)}{2(q-2)}\frac{1-\frac{2}{3}\beta}{1-\beta}\left(\frac{v}{\sigma}\right)^2\right)^{q/1-q},\qquad 1<q<2. \tag{7}$$

The corresponding two-dimensional M-B distribution with asymmetry β is given by

$$f_{\rm MB}(v,\beta,\sigma)=\frac{1-\frac{2}{3}\beta}{2\pi(1-\beta)\sigma^2}\exp\left(-\frac{(1-\frac{2}{3}\beta)v^2}{2(1-\beta)\sigma^2}\right). \tag{8}$$

This can be obtained from Eq. (7) in the limit $q\to 1$. As explained earlier, we assumed $q=3/4$ for f_r and $q=5/3$ for f_t for the more realistic VDF, which implies that the range of allowed velocities is $v<3\sigma/\sqrt{1-(2/3)\beta}$, which is slightly different from the relation $v<2.84v_0\approx 4\sigma$ normally imposed on the M-B distribution. The shapes of the two 2-dimensional tangential velocity distributions are shown together in Fig. 2 and exhibit substantial differences in the width and the attained maximum, as well as at high velocities. Note that the factor $2\pi v$ is just from the 2-dimensional phase-space volume.

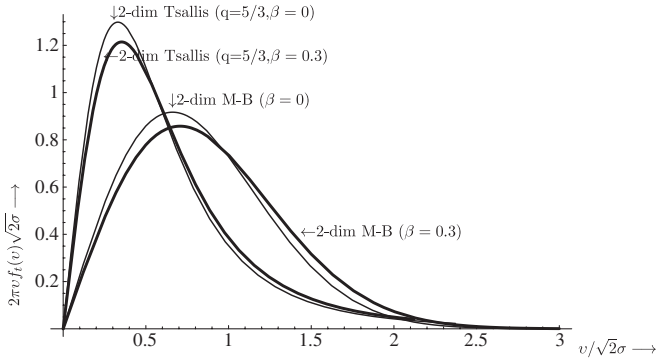

FIG. 2. The 2-dimensional Tsallis and M-B normalized tangential velocity distributions $2\pi v f_t(v)$ are shown as functions of $v/\sigma\sqrt{2}$ ($v=v_t$) for values of the asymmetry parameter $\beta=0$ (thick line) and $\beta=0.3$ (fine line). The Tsallis curves with $q=5/3$ are the ones reaching the highest maximum value at lower velocity.

In terms of β and σ the radial velocity distributions are

$$f_r(v,\beta,\sigma)=\frac{35\sqrt{1-\frac{2}{3}\beta}\left(1-\frac{v^2(1-(2\beta/3))}{9\sigma^2}\right)^3}{96\sigma}\quad\text{(Tsallis function, } q=3/4), \tag{9}$$

and

$$f_r(v,\beta,\sigma)=\frac{e^{-(v^2(1-(2\beta/3))/2\sigma^2)}\sqrt{1-\frac{2\beta}{3}}}{\sqrt{2\pi}\sigma}\text{(MB)}. \tag{10}$$

We note that in the case of the M-B distribution $\sigma=v_0/\sqrt{2}$, where v_0 is the Sun's rotational velocity. In the case of the Tsallis functions considered here, one has $\langle v^2\rangle=3\sigma^2$ for all q. We impose the condition $\langle v^2\rangle=(3/2)v_0^2$ (as for the M-B distribution) even for $q\neq 1$ which implies $\sigma=v_0/\sqrt{2}$.

III. THE DIRECT DETECTION EVENT RATE

We will now calculate both the total detection rate and the annual modulation rate. However, before computing the detection event rate it is necessary to transform the distributions from the galactic to the local coordinate system.

From the kinematics of the WIMP-nucleus collision one has that the momentum transfer to the nucleus is given by

$$q=2\mu_r v\xi, \tag{11}$$

where ξ is the cosine of the angle between the WIMP velocity and the momentum of the outgoing nucleus, and μ_r is the reduced mass of the system. Instead of the variable ξ one can introduce the energy Q transferred to the nucleus, $Q=q^2/(2Am_p)$, where Am_p is the nuclear mass. Thus

$$2\xi d\xi=\frac{Am_p}{2(\mu_r v)^2}dQ.$$

Furthermore, for a given energy transfer the velocity v is constrained to be

$$v\geq v_{\rm min},\qquad v_{\rm min}=\sqrt{\frac{QAm_p}{2}}\frac{1}{\mu_r}. \tag{12}$$

We will find it convenient to introduce, instead of the energy transfer, the dimensionless quantity u

$$u=\frac{1}{2}(qb)^2\equiv\frac{Q}{Q_0},\qquad Q_0=\frac{1}{Am_pb^2}=4.1\times 10^4A^{-4/3}\ \text{keV}, \tag{13}$$

where b is the nuclear (harmonic oscillator) size parameter.

It is therefore clear that for a given energy transfer the velocity is restricted from below, and we have already mentioned that the velocity is bounded from above by the escape velocity. We introduce a normalized velocity by the dimensionless variable

$$y = v/(\sigma\sqrt{2}), \qquad a\sqrt{u} \le y \le y_{\rm esc}, \tag{14}$$

with $a = (2\mu_r b\sigma)^{-1}$. Thus,

$$\xi d\xi = \frac{a^2}{y^2} dy. \tag{15}$$

The event rate for the coherent WIMP-nucleus elastic scattering is given by [31]

$$R = \frac{\rho(0)}{m_{\chi^0}} \frac{m}{m_p} \sqrt{\langle v^2 \rangle} f_{\rm coh}(A, \mu_r(A)) \sigma^S_{p,\chi^0}, \tag{16}$$

or, using typical numerical values,

$$R \simeq 1.6010^{-3} \frac{t}{1\ \text{y}} \frac{\rho(0)}{0.3\ \text{GeV cm}^{-3}} \frac{m}{1\ \text{kg}} \frac{\sqrt{\langle v^2 \rangle}}{280\ \text{kms}^{-1}} \times \frac{\sigma^S_{p,\chi^0}}{10^{-6}\ \text{pb}} f_{\rm coh}(A, \mu_r(A)). \tag{17}$$

Here, σ^S_{p,χ^0} is the WIMP-nucleon scalar cross section, $\rho(0)$ is the WIMP density in our vicinity, m_{χ^0} is the WIMP mass, m is the target mass, A is the number of nucleons in the nucleus, $\langle v^2 \rangle = 3v_0^2/2$ is the root-mean-square WIMP velocity. The dimensionless quantity $f_{\rm coh}(A, \mu_r(A))$ is given by

$$f_{\rm coh}(A, \mu_r(A)) = \frac{100\ \text{GeV}}{m_{\chi^0}} \left[\frac{\mu_r(A)}{\mu_r(p)}\right]^2 A t_{\rm coh}(1 + h_{\rm coh} \cos\alpha). \tag{18}$$

The quantity of interest to us is $r = t_{\rm coh}(1 + h_{\rm coh}\cos\alpha)$, which is also dimensionless. The angle α describes the position of the Earth in its solar orbit. This can be viewed as a ''relative'' rate and contains all the information regarding the WIMP velocity distribution and the structure of the nucleus. It also depends on the reduced mass of the system.

The event rate is proportional to the WIMP flux, i.e. proportional to the WIMP velocity. It is not difficult to show [31] that

$$\frac{dr}{du} = F^2(u) \int_{a\sqrt{u}}^{y_{\rm esc}} \sqrt{\frac{2}{3}} y \frac{a^2}{y^2} y^2 dy \int_0^{\pi} d\theta \int_0^{2\pi} d\phi f_r(y, \theta) \times f_t(y, \theta, \phi, \alpha) \Theta(y^2_{\rm esc} - f_b), \tag{19}$$

with $F(u)$ the nuclear form factor. In the integrand we have explicitly displayed all the factors of y in order to keep track of their origin. The first one comes from the WIMP flux, the second from the transformation (15) and the last is the usual phase-space factor. $\Theta(x)$ is the Heaviside function introduced to guarantee that the WIMP velocity is bounded by the escape velocity. Thus,

$$f_b = y^2 + y_0^2 + \delta_0^2 + y_0\delta_0 \cos\alpha + 2y\delta_0 \cos\theta \sin\alpha.$$

Even though the values of $y_{\rm esc}$ are different, the effect of this constraint is small, with the possible exception of the event rates for very high threshold energy. In that special case the difference in the upper cutoff, $y_{\rm esc}$, between the two models may yield significant differences.

This way the differential event rate in Eq. (19) can be cast in the form

$$\frac{dr}{du} = \sqrt{\frac{2}{3}} a^2 F^2(u) \Psi(a\sqrt{u}, \alpha). \tag{20}$$

We have seen that the parameter a depends on the nucleus, the velocity distribution (v_0 or σ) and the WIMP mass.

By performing a Fourier analysis of the function $\Psi(x, \alpha)$, which is a periodic function of α, and keeping the dominant terms we find

$$\frac{dr}{du} = \sqrt{\frac{2}{3}} a^2 F^2(u) \Psi_0(a\sqrt{u})[1 + H(a\sqrt{u}) \cos\alpha]. \tag{21}$$

Sometimes we will consider each term separately in the above expression by writing

$$\begin{aligned} \frac{dr}{du} &= \frac{dt}{du} + \frac{d\tilde{h}}{du} \cos\alpha, \\ \frac{dt}{du} &= \sqrt{\frac{2}{3}} a^2 F^2(u) \Psi_0(a\sqrt{u}), \\ \frac{d\tilde{h}}{du} &= \sqrt{\frac{2}{3}} a^2 F^2(u) \Psi_0(a\sqrt{u}) H(a\sqrt{u}) \end{aligned} \tag{22}$$

It is thus clear, that Ψ_0 and t are related to the total rates, whereas H and h are related to the annual modulations.

Before proceeding further by considering a special target, it is instructive to concentrate on $\Psi_0(x)$ and the modulation $H(x)$ as functions of the asymmetry parameter β. For this purpose we show the function $\Psi_0(x)$ in Fig. 3 and the function $H(x)$ in Fig. 4. In the case of $\Psi_0(a\sqrt{u})$, one clearly sees that the effect of the asymmetry parameter β is small for all energy transfers. In the case of the M-B distribution one has that larger β implies a smaller differential rate, while in the case of the more realistic distribution a larger asymmetry implies a larger differential rate. In both cases the function $H(a\sqrt{u})$ is an increasing function of $a\sqrt{u}$ accompanied by a change in sign. Thus in obtaining the modulation of the total amplitude the contribution of the low Q section tends to cancel the high Q part. Which part will dominate depends on the reduced mass and the nuclear form factor. In the case of the present realistic distribution, the velocity asymmetry has a small effect on the modulation of the differential rate, and this effect occurs at high energy transfers.

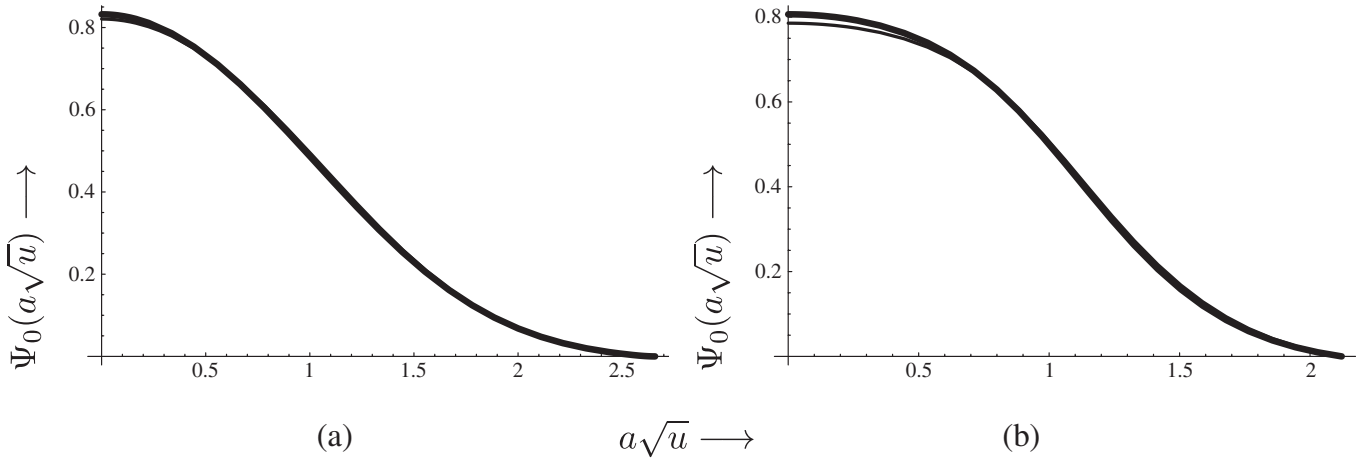

FIG. 3. The time-independent part of the differential rate, $\Psi_0(a\sqrt{u})$, as a function of the energy transfer $a\sqrt{u}$. The normally used M-B distribution is on the left and the present realistic velocity distribution is on the right. There is essentially no dependence on the velocity asymmetry parameter.

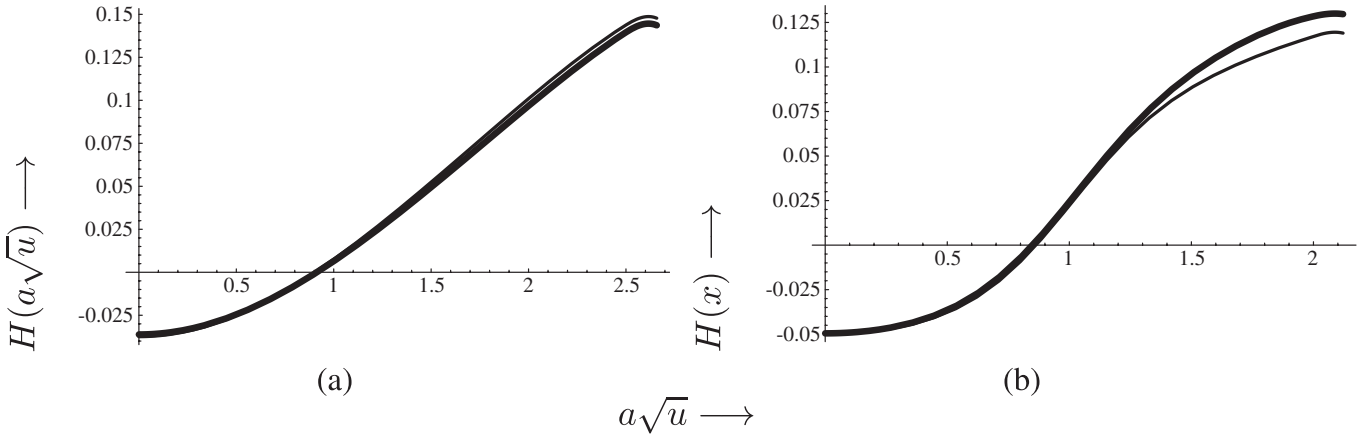

FIG. 4. The same as in Fig. 3 for the function $H(a\sqrt{u})$, which describes the coefficient of the time-dependent part of the differential rate (differential modulated amplitude). Note the change in sign as $a\sqrt{u}$, i.e. the energy transfer, increases. This leads to cancellations in the total modulation amplitude. M-B is on the left, Tsallis is on the right. In some cases it may even become negative (maximum event rate in December). The dependence on the asymmetry is small, visible only at high energy transfers.

IV. APPLICATIONS

Let us now focus on the aspects affected by the WIMP velocity distribution. The total (time-averaged) rate is given by

$$t_{\rm coh} = \int_{u_{\rm min}}^{u_{\rm max}} \frac{dt}{du} du, \tag{23}$$

where $u_{\rm min}$ is determined by the detector threshold and $u_{\rm max} = (y_{\rm esc})^2/a^2$ by the maximum WIMP velocity. By including both $\Psi_0(a\sqrt{u})$ and $H(a\sqrt{u})$ we can cast the rate in the form

$$\begin{aligned} r_{\rm coh} &= t_{\rm coh}(1 + h_{\rm coh}\cos\alpha), \\ h_{\rm coh} &= \frac{1}{t_{\rm coh}} \int_{u_{\rm min}}^{u_{\rm max}} \frac{d\tilde{h}_{\rm coh}}{du} du, \end{aligned} \tag{24}$$

where the dimensionless quantity r characterizes the total rate, and h is the annual modulation.

The direct WIMP detection rate depends on the nucleus via its form factor and its mass. It also depends on the WIMP mass through the reduced mass μ_r, entering through the parameter a. For our numerical study we will focus on two very different targets to show general trends, namely, a medium heavy target, ^{127}I, and a light one, ^{19}F, which are two of the most popular targets employed.

A. The case of a light target

The actual results have been obtained for ^{19}F, but those of other light targets are similar. The nuclear form factor we use was obtained in the shell model description of the target and is shown in Fig. 5. Integrating over the energy transfer, assuming either no detector cutoff ($u_{\rm min} = 0$) or a

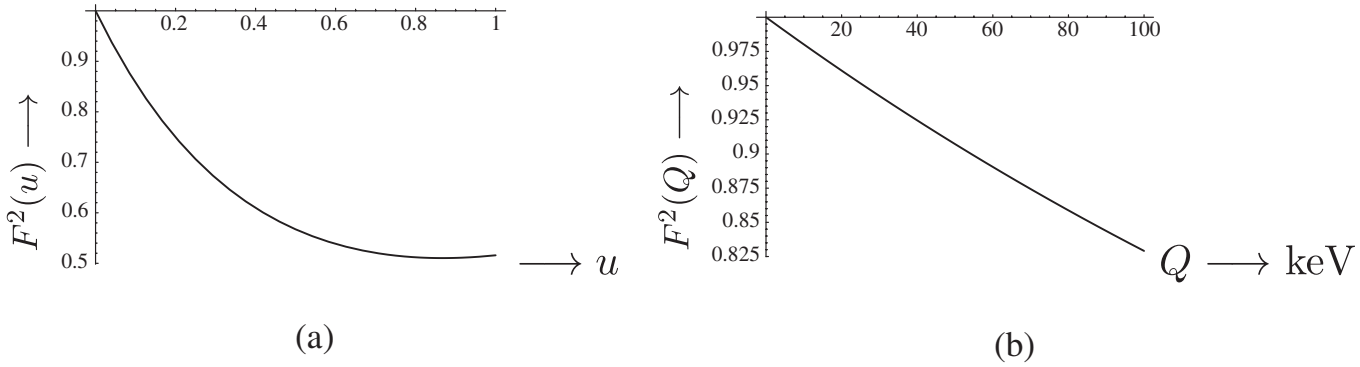

FIG. 5. (a) The form factor $F^2(u)$ for ^{19}F employed in our calculation as a function of $u = Q/Q_0$, where Q is the energy transfer to the nucleus and $Q_0 = 809$ keV. (b) The same quantity as a function of the energy transfer Q.

cutoff of $Q_{\text{thr}} = 5$ keV, we obtain the total rate in the case of the target ^{19}F. The results are shown in Fig. 6 for t and in Fig. 7 for h.

B. The case of an intermediate mass target

Even though the actual results have been obtained for ^{127}I, the situation is similar for other intermediate targets.

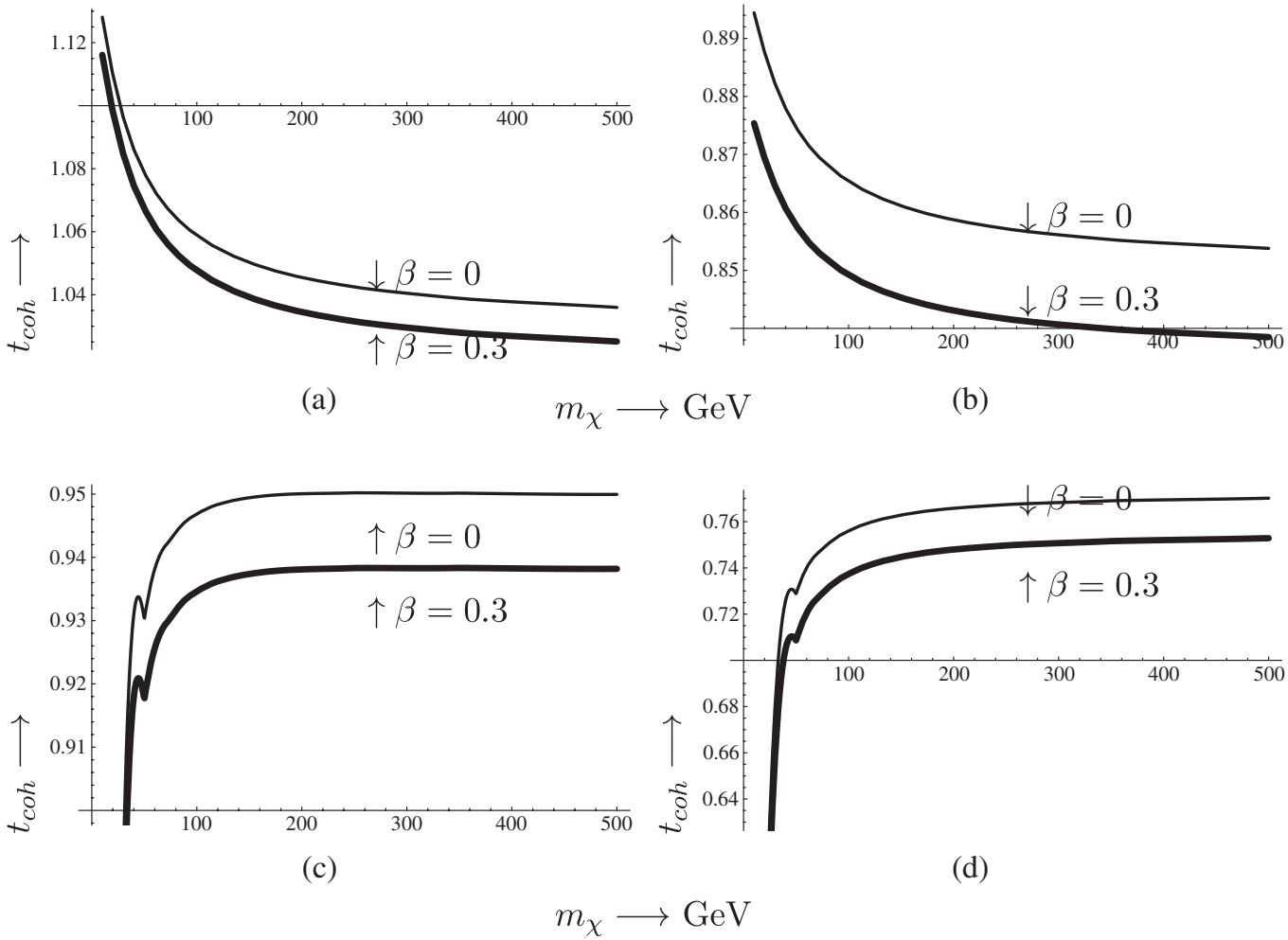

FIG. 6. The dimensionless quantity t_{coh} in the case of the target ^{19}F for $Q_{\text{thr}} = 0$ at the top and $Q_{\text{min}} = 5$ keV at the bottom. The abscissa is for different WIMP masses, m_χ. t_{coh} represents the time-independent part of the detection rate. On the left are the results obtained for a M-B distribution, while on the right those for the more realistic distribution. The thick and thin curves correspond to $\beta = 0$ and 0.3, respectively.

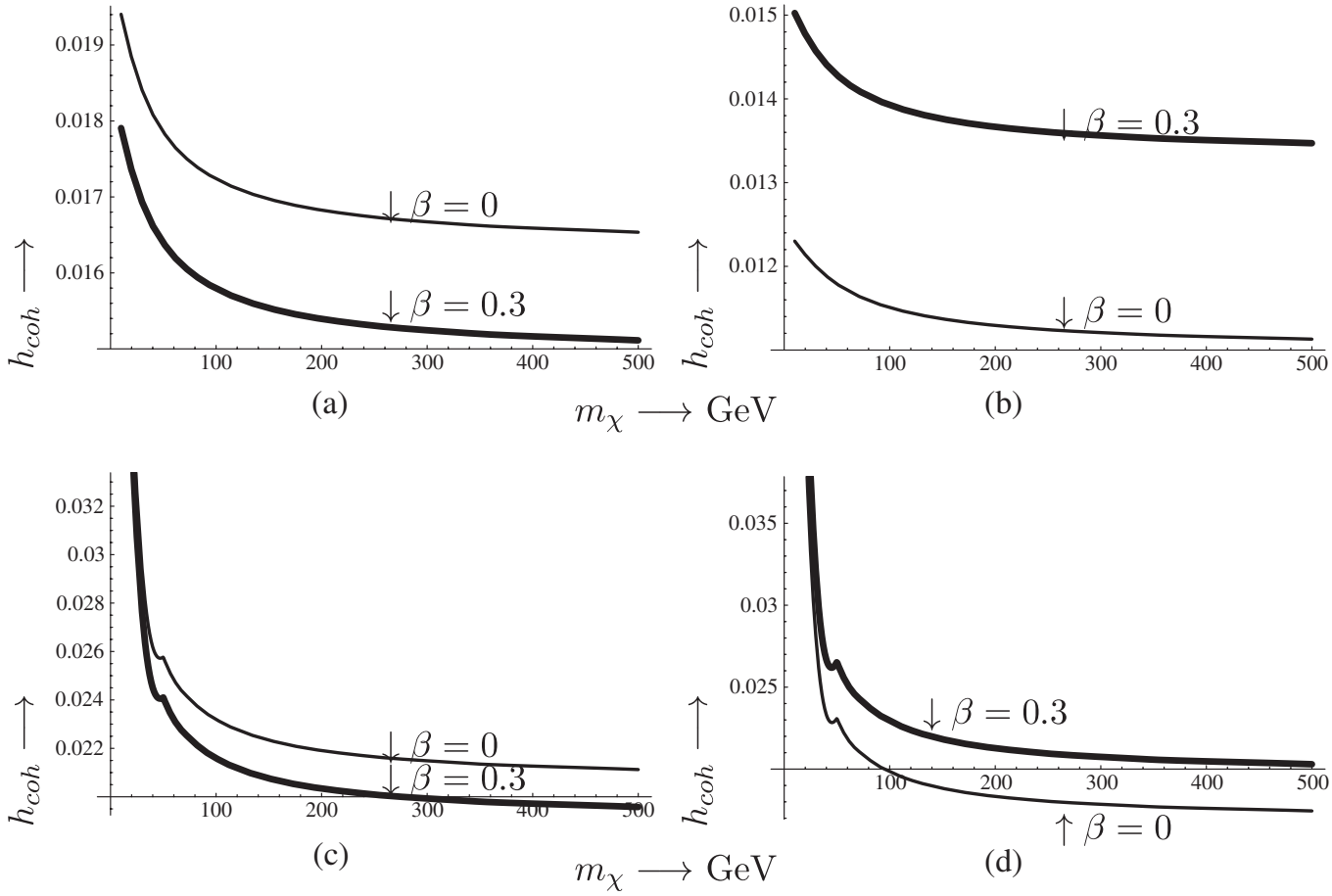

FIG. 7. The same as in Fig. 6 for the quantity $h_{\rm coh}$, which represents the time-dependent part of the detection rate (the annual modulation).

The nuclear form factor employed was obtained in the shell model description of the target and is shown in Fig. 8. In the case of the target ^{127}I the obtained results are shown in Figs. 9 and 10 for $Q_{\rm min} = 0$ at the top and $Q_{\rm min} = 10$ keV at the bottom.

V. DISCUSSION

In our formalism the quantities which are affected by the velocity distribution, are the parameters t, describing the total time-averaged rate, and h describing the amplitude of the time-dependent rate (modulation effect). These parameters also depend on the target nucleus as well as the WIMP mass. In this work they have been obtained in the case of the coherent scattering, but they are not expected to be very different in the case of the spin mode. Our results can be summarized as follows:

(1) *The time average rate.*—The parameter $t_{\rm coh}$ in the case of symmetric velocity distribution ($\beta = 0$) is

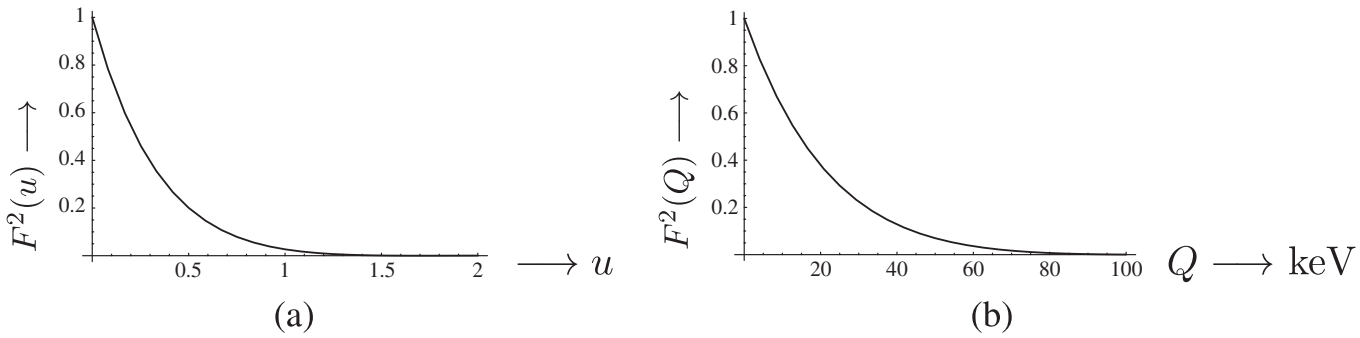

FIG. 8. (a) The form factor $F^2(u)$ for ^{127}I employed in our calculation as a function of $u = Q/Q_0$, where Q is the energy transfer to the nucleus and $Q_0 = 64$ keV. (b) The same quantity as a function of the energy transfer Q.

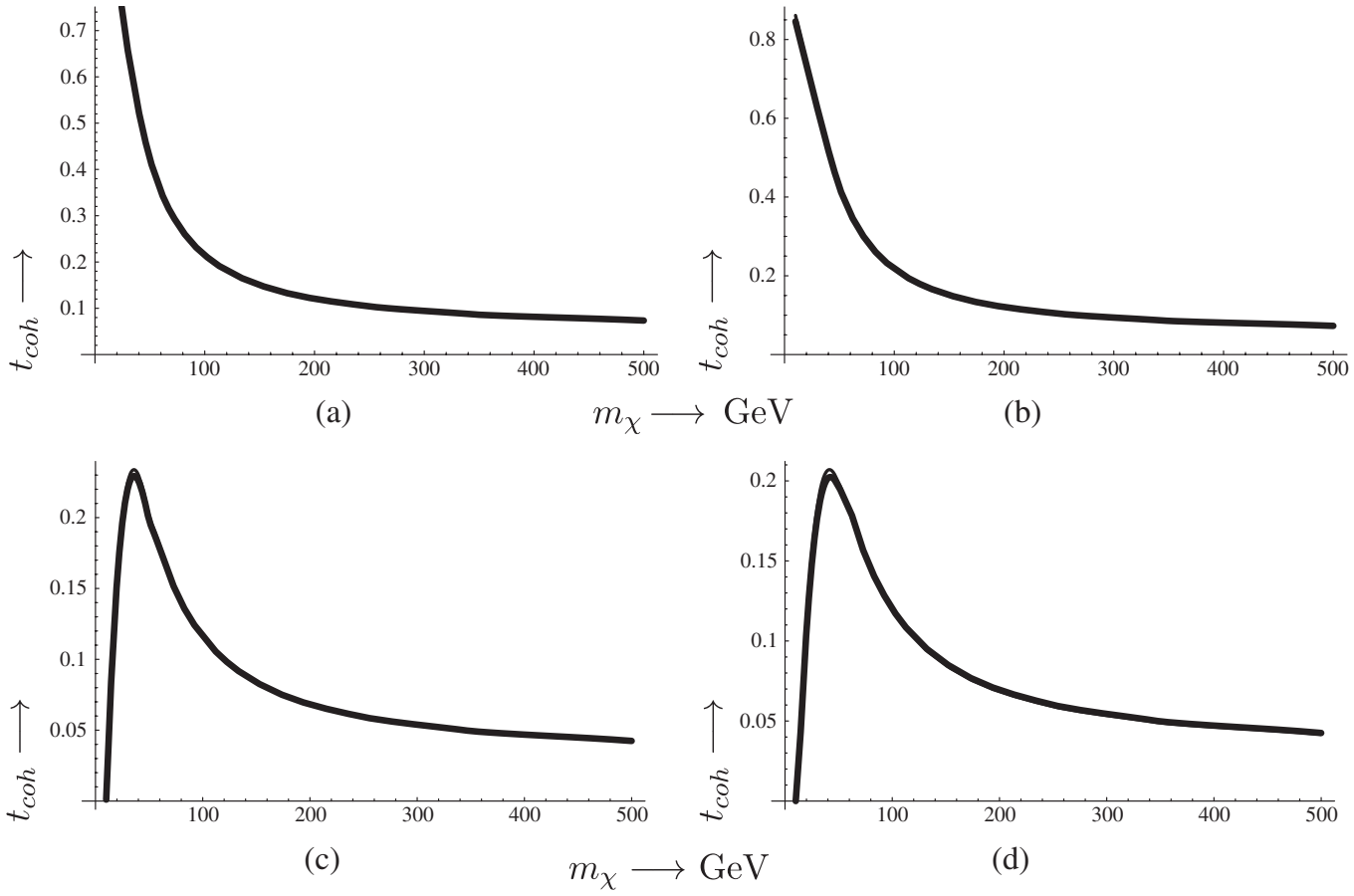

FIG. 9. The same as in Fig. 6 in the case of the target ^{127}I. Now at the bottom the results shown correspond to $Q_{\rm thr} = 10$ keV. The dependence on the asymmetry parameter β is not visible.

not very different from that obtained in various other models, like those obtained in the Eddington approach [19–22]. The obtained results depend on the choice of the target. Thus,

(a) *The parameter t for a light target.*—It is at first a decreasing function of the WIMP mass and eventually becomes a constant for heavy WIMPs, which for the realistic VDF is approximately 20% lower than for the M-B case. This limiting value is not much affected by threshold effects. The value of the parameter t at low WIMP masses is, as expected, sensitive to the attained energy threshold. The dependence on the asymmetry parameter is small (few percent) in both distributions.

(b) *The parameter t for a heavy target.*—The general behavior is similar to the above except that now the limiting value is an order of magnitude lower. This may partly offset the advantages offered by the favorable nuclear mass dependence of the event rate, which is proportional to $\sim \mu_r^2 A \approx A^3$ [see Eqs. (16)–(18)], not included in the plots. A threshold of 10 keV further reduces the rate by about a factor of 2. At low WIMP mass the advantage of employing an intermediate target is expected, since t is only about a factor of 3 down from that of a light target. The effect of the realistic VDF is small (from a few to 10%). The effect of asymmetry is close to unobservable.

(2) *The modulation effect.*—We can now focus on two issues:

(a) *The modulation of the differential rate.*—All the previous velocity distributions imply a modulation amplitude which (i) increases with energy transfer, and (ii) changes sign as we go from low to high energy transfers. Also, (iii) the slope and the point of the change of sign depend on the WIMP mass and the nature of the target.
In the case of the present realistic velocity all the above hold true. The effect of the velocity asymmetry is quite small.

(b) *The total modulation amplitude.*—
(i) In the case of a light target both distri-

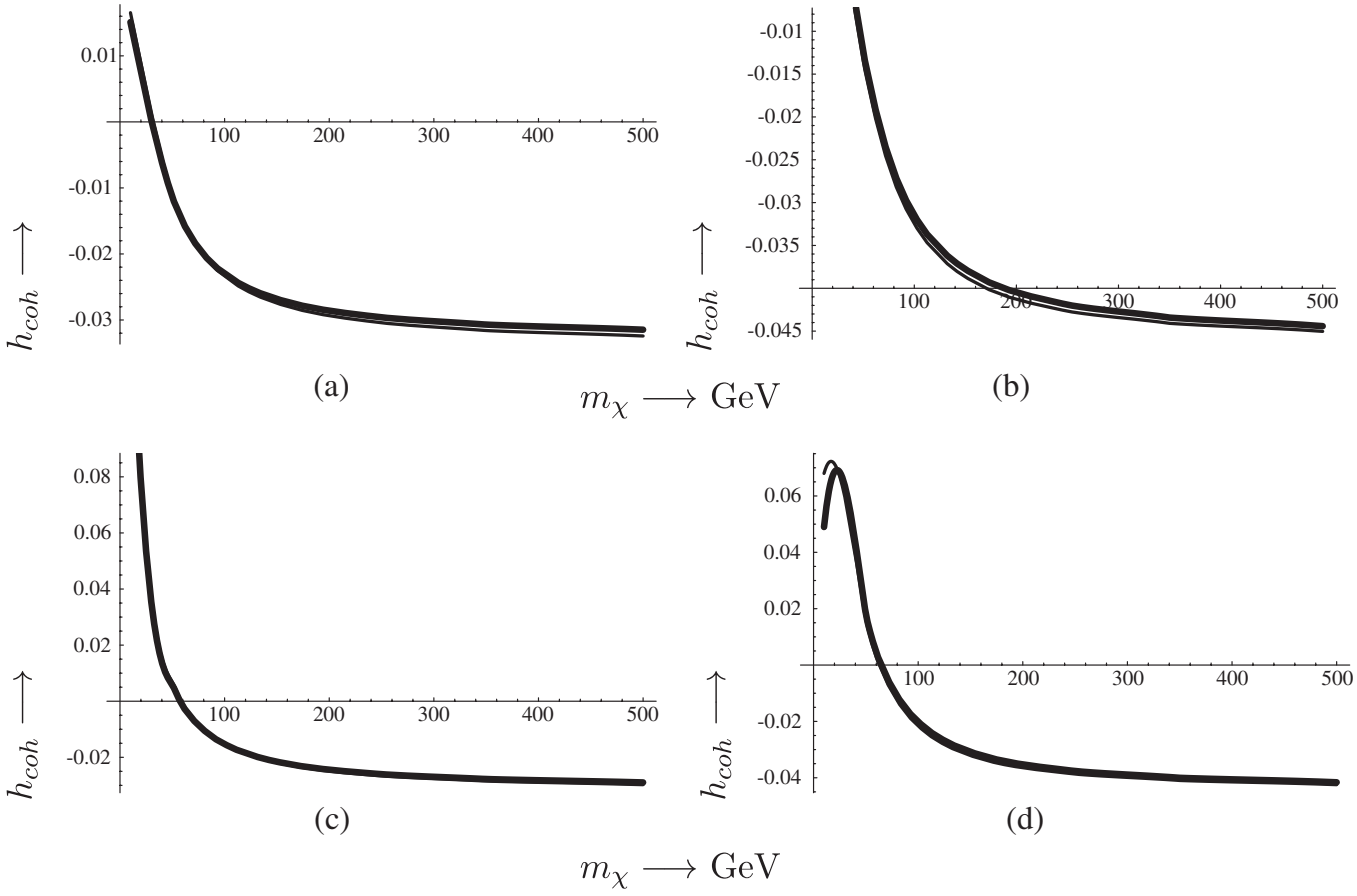

FIG. 10. The same as in Fig. 9 in the case of $h_{\rm coh}$. The dependence on the asymmetry parameter β is barely visible.

butions predict a similar modulation amplitude. Its sign is positive, i.e. the maximum is around June 3rd. The effect of asymmetry is small, but, when comparing the two models, it tends to go in opposite directions. Unfortunately the predicted difference between the maximum and the minimum at zero threshold cannot exceed 4%. It may double for an energy threshold of about 5 KeV.

(ii) In the case of a heavy-intermediate target, the modulation becomes negative for both models as the WIMP mass increases. Thus the event rate for both models may attain a maximum in December. The difference between the maximum and the minimum is now quite a bit higher, i.e. it can be as high as 9% depending on the WIMP mass. For a light WIMP mass the modulation is quite small at zero threshold. In the presence of energy thresholds it tends to increase. This is understandable, since the modulation here is the ratio of two quantities [see Eq. (24)] and the denominator, which determines the average event rate, falls much faster then the numerator in the presence of a threshold. The modulation can be quite sizable, especially for light WIMPs. With a 10 keV threshold we predict differences between maximum and minimum of about 5%–15% in the case of both a M-B distribution and the present distribution. The event rate may attain a maximum in June for light WIMPs. The effect of the velocity asymmetry is virtually negligible.

VI. CONCLUSIONS

The event rate for direct WIMP detection depends on the nucleon cross section (which in turn depends on the assumed particle model), the WIMP mass, the structure of the target, and the WIMP velocity distribution. In the present study we focused on the last aspect by considering a realistic velocity distribution similar to the ones extracted

from numerical N-body simulations, here parametrized by the Tsallis shape. Generally speaking, the calculations using the M-B distribution and the present distribution yield similar results. This is particularly true of the time-independent part of the event rate. Some differences show up, however, in the prediction of the time-dependent event rate, described by the modulation amplitude h (the difference between the maximum and the minimum event rates being $2|h|$). For intermediate mass targets at zero energy threshold the modulation amplitude obtained in the present calculation is small for light WIMPs, $|h| < 2\%$, but it can reach values of $|h| \approx 5\%$ for heavy WIMPs. For light WIMPs in the presence of an energy threshold of a few keV the obtained values of $|h|$ may become larger, but this occurs at the expense of the number of counts. The predicted effect on the event rates of the asymmetry parameter of the velocity distribution is relatively small.

It will be interesting to explore the possible consequences of the realistic velocity distribution considered in this work on the event rates of experiments which measure the direction of the recoiling nucleus [32–34].

ACKNOWLEDGMENTS

S. H. H. would like to thank Nicolao Fornengo and Stefano Scopel for early encouraging discussions. J. D. V. would like to thank the European Network of Theoretical Astroparticle Physics ENTApP ILIAS/N6 under Contract No. RII3-CT-2004-506222 for financial support. The Dark Cosmology Centre is funded by the Danish National Research Foundation.

[1] D. N. Spergel *et al.*, Astrophys. J. Suppl. Ser. **148**, 175 (2003).
[2] D. N. Spergel *et al.*, Astrophys. J. Suppl. Ser. **170**, 377 (2007); L. Page *et al.*, *ibid.* **170**, 335 (2007); G. Hinshaw *et al.*, *ibid.* **170**, 288 (2007); N. Jarosik *et al.*, *ibid.* **170**, 263 (2007).
[3] M. W. Goodman and E. Witten, Phys. Rev. D **31**, 3059 (1985).
[4] T. S. Kosmas and J. D. Vergados, Phys. Rev. D **55**, 1752 (1997).
[5] J. Ellis and L. Roszkowski, Phys. Lett. B **283**, 252 (1992).
[6] A. Bottino *et al.*, Phys. Lett. B **402**, 113 (1997); P. Nath and R. Arnowitt, Phys. Rev. Lett. **74**, 4592 (1995); R. Arnowitt and P. Nath, Phys. Rev. D **54**, 2374 (1996); **60**, 044002 (1999); V. A. Bednyakov, H. V. Klapdor-Kleingrothaus, and S. G. Kovalenko, Phys. Lett. B **329**, 5 (1994).
[7] J. D. Vergados, J. Phys. G **22**, 253 (1996).
[8] M. T. Ressell and D. J. Dean, Phys. Rev. C **56**, 535 (1997).
[9] P. C. Divari, T. S. Kosmas, J. D. Vergados, and L. D. Skouras, Phys. Rev. C **61**, 054612 (2000).
[10] A. K. Drukier, K. Freese, and D. N. Spergel, Phys. Rev. D **33**, 3495 (1986); J. I. Collar *et al.*, Phys. Lett. B **275**, 181 (1992).
[11] J. D. Vergados, Phys. Rev. D **62**, 023519 (2000).
[12] N. Evans, M. Carollo, and P. Zeeuw, Mon. Not. R. Astron. Soc. **318**, 1131 (2000).
[13] N. Fornengo and S. Scopel, Phys. Lett. B **576**, 189 (2003).
[14] S. H. Hansen and B. Moore, New Astron. Rev. **11**, 333 (2006); S. H. Hansen and J. Stadel, J. Cosmol. Astropart. Phys. 05 (2006) 014.
[15] O. Host and S. H. Hansen, J. Cosmol. Astropart. Phys. 06 (2007) 016.
[16] S. H. Hansen and R. Piffaretti, Astron. Astrophys. **476**, L37 (2007).
[17] C. Copi, J. Heo, and L. Krauss, Phys. Lett. B **461**, 43 (1999).
[18] A. M. Green, Phys. Rev. D **66**, 083003 (2002).
[19] A. S. Eddington, Mon. Not. R. Astron. Soc. **76**, 572 (1916).
[20] P. Ullio and M. Kamioknowski, J. High Energy Phys. 03 (2001) 049.
[21] J. D. Vergados and D. Owen, Phys. Rev. D **75**, 043503 (2007).
[22] P. Belli, R. Cerulli, N. Fornengo, and S. Scopel, Phys. Rev. D **66**, 043503 (2002).
[23] N. Tetradis, J. D. Vergados, and A. Faessler, Phys. Rev. D **75**, 023504 (2007).
[24] C. Tsallis, J. Stat. Phys. **52**, 479 (1988).
[25] S. H. Hansen, M. Zemp, B. Moore, and J. Stadel, J. Cosmol. Astropart. Phys. 01 (2006) 014.
[26] S. H. Hansen, D. Egli, L. Hollenstein, and C. Salzmann, New Astron. Rev. **10**, 379 (2005).
[27] N. W. Evans and J. H. An, Phys. Rev. D **73**, 023524 (2006).
[28] J. F. Navarro, C. S. Frenk, and S. White, Astrophys. J. **462**, 563 (1996).
[29] A. W. Graham, D. Merritt, B. Moore, J. Diemand, and B. Tersić, Astron. J. **132**, 2701 (2006).
[30] E. Salvador-Solé, A. Manrique, G. González-Casado, and S. H. Hansen, Astrophys. J. **666**, 181 (2007).
[31] J. D. Vergados, Phys. Rev. D **63**, 063511 (2001); Phys. Rev. D **67**, 103003 (2003); Lect. Notes Phys. **720**, 69 (2007); J. Phys. G **30**, 1127 (2004).
[32] B. Morgan, A. M. Green, and N. J. C. Spooner, Phys. Rev. D **71**, 103507 (2005).
[33] J. D. Vergados and Amand Faessler, Phys. Rev. D **75**, 055007 (2007).
[34] N. Spooner, arXiv:0705.3345.